Efficient uncertainty analysis method for structures with hybrid uncertainty based on reduced-order model

Luyi Li
Professor, School of Aeronautics, Northwestern Polytechnical University, Xi'an, China

Zeming Chang
PhD student, School of Aeronautics, Northwestern Polytechnical University, Xi'an, China

ABSTRACT: An efficient uncertainty analysis method is proposed in this paper for structures with hybrid random and interval variables by using the idea of reduced-order model. In the proposed method, proper orthogonal decomposition (POD) is firstly employed to extract the optimal orthogonal bases, which are the most characteristic structure functions, from the hybrid uncertainty space based on a set of selected full hybrid uncertainty analysis. Due to the existence of the hybrid uncertainty, the truncated orthogonal bases of the POD are functions of the random variables with unknown coefficients being functions of the interval variables. Kriging model is then used to approximate these unknown coefficients to improve the computational efficiency. Combined with the model reduction ability of POD and the efficiency of the Kriging model, the proposed method provides an efficient reduced-order model for full uncertainty propagation of hybrid random and interval uncertainty. Furthermore, due to the complete decoupling of the random and interval effect, the proposed method avoids repeated random uncertainty analysis at each realization of the interval variables, and significantly improves the efficiency of hybrid uncertainty analysis. Two test examples demonstrate that the proposed method significantly reduces the computational cost that arise due to high-dimensional random and interval variables, while demonstrating a similar accuracy for predicting the response bounds as the full-order hybrid uncertainty analysis.

With the developments of structure and system complexity, it has been widely recognized that uncertainty plays a crucial role in engineering analysis, design and decision-making activities [1]. Uncertainty analysis (UA) can quantify various uncertainties in the input parameters of the structures and systems, and evaluate their influence on the output performance or behavior. At present, there are two main techniques for uncertainty analysis: probabilistic technique and non-probabilistic technique. In the probabilistic framework, random model is often used to quantify uncertainty. Based on random model, a variety of probabilistic analysis methods have been developed, such as Monte Carlo simulation (MCS) method [2], perturbation stochastic method [3], surrogate model method [4] and so on, which have received extensive investigation in the field of UA. However, in probabilistic studies, a large number of statistical data is required to determine the precise probability distributions of uncertain parameters. If the available data is limited or even scarce, probabilistic method will be powerless.

To this end, non-probabilistic technique is developed, and many different non-probabilistic models, such as interval model, fuzzy set model and evidence model have been proposed to quantify uncertainty according to the information available. Among these non-probabilistic models, interval model is one of the most widely used one due to its modeling convenience, in which uncertainty is processed by interval variables with given lower and upper bounds. Besides, many other non-probabilistic models can be seen as extensions of the interval model. Based on the interval model, various non-probabilistic methods have been proposed to conduct interval analysis for real-world problems and response prediction, such as vertex combination method [5], interval

perturbation method [6], interval optimization method [7] and recently developed sequential simulation method [8].

In practical engineering, hybrid random and interval uncertainties normally coexist in a complex system. Therefore, many hybrid UA methods have been developed, which aim at addressing this complex situation by integrating the merits of random and interval theories. With the help of the random and interval theories, a mixed perturbation Monte-Carlo method is proposed in Ref. [9] for hybrid probabilistic interval analysis of bar structures. A perturbation vertex method is developed in [10] to deal with the structural-acoustic problem with hybrid probabilistic and non-probabilistic uncertainties. An UA approach based on polynomial chaos expansion method is put forward in [11] for hybrid UA of the composite structures. Besides, a number of hybrid UA methods [12][13] also have been developed for systems subjected to P-box uncertainties, where the probabilistic distribution of random variable is considered to be bracketed in an interval. Although a large amount of research is currently available for hybrid UA, it should be noted that the existing methods for hybrid uncertainty problems with both random and interval variables are mainly based on the MCS, perturbation technique, optimization technique or polynomial chaos theory. Advanced research is still in need to further improve the efficiency of accuracy of the hybrid random and interval UA.

In the field of UA, surrogate modeling methods have played a significant role in decreasing the cost of the large-scale and high-fidelity simulations, which aim at finding inexpensive approximations of the system's input-output relation. Nevertheless, for problems with high-dimensional physical space, constructing a surrogate model is still computationally challenging due to the large number of spatial degrees of freedom (DOF). To this end, reduced-order modeling (ROM) method is proposed, which aims at constructing a low-dimensional representation of the simulation's responses defined on a basis which optimally spans the simulation's output space [14]. At present, ROM method has been widely used in many fields of science and engineering, such as fluid and structural mechanics [15][16]. For structural systems involving both random and interval uncertainty, system behaviors at different realizations of the interval variables often are correlated. Therefore, it is possible to establish a low-dimensional representation of all the system's output with a much smaller number of simulation outputs. Based on this idea, the aim of this paper is to extend ROM method for hybrid UA problems with both random and interval variables.

1. UA FOR STRUCTURES WITH HYBRID RANDOM AND INTERVAL UNCERTAINTY

For the structures or systems with both random and interval variables, the response function can be expressed as

$$Y = g(\boldsymbol{X}, \boldsymbol{Z}) \tag{1}$$

where $\boldsymbol{X}=\left[X_1,...,X_{n_R}\right]^{\mathrm{T}}$ is n_R-dimensional random vector with the joint probability density function (PDF) $f_{\boldsymbol{X}}(\boldsymbol{x})$ or joint cumulative distribution function (CDF) $F_{\boldsymbol{X}}(\boldsymbol{x})$, $\boldsymbol{Z}=\left[Z_1,...,Z_{n_I}\right]^{\mathrm{T}}$ is n_I-dimensional interval vector with each $Z_i=\left[Z_i^{\mathrm{L}},Z_i^{\mathrm{U}}\right]$, where Z_i^{L} and Z_i^{U} are the lower and upper bounds of Z_i respectively. Therefore, $\boldsymbol{Z}$ varies in a compact set Ω of $\mathbb{R}^{n_I}$. Y is the output response.

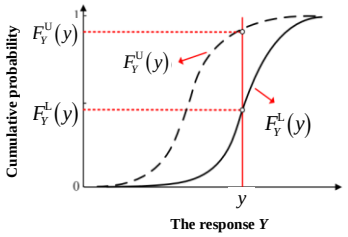

Figure 1: The P-box of the response Y

Under the combined action of random and interval variables, the response Y has the properties of both random and interval variables and is an interval random variable. The uncertainty of Y can be represented by a P-box

which is delimited by the lower and upper boundaries of the CDF of *Y*, as shown in Figure 1.

In Figure 1, $F_Y^{\mathrm{L}}(y)$ and $F_Y^{\mathrm{U}}(y)$ are the lower and upper boundaries of the CDF of *Y*, respectively. Based on the P-box of *Y*, the statistical characteristics of *Y*, such as expectation and variance, are interval variables. Take the expectation as illustration, it can be obtained by

$$\mu_Y = \left[\mu_Y^{\mathrm{L}}, \mu_Y^{\mathrm{U}}\right] = \left[\int y f_Y^{\mathrm{L}}(y)dy, \int y f_Y^{\mathrm{U}}(y)dy,\right] \quad (2)$$

where $f_Y^{\mathrm{L}}(y)$ and $f_Y^{\mathrm{U}}(y)$ are the derivatives of $F_Y^{\mathrm{L}}(y)$ and $F_Y^{\mathrm{U}}(y)$ respectively.

The purpose of the hybrid random and interval UA is to obtain P-box of *Y*, and the intervals of its statistical characteristics. To this end, many approaches have been proposed in the literature, such as the hybrid perturbation Monte Carlo method [9] and hybrid perturbation vertex method [10]. However, most of the existing studies mainly focused on the evaluation of the expectations and variances of system responses.

2. HYBRID UA BASED ON REDUCED-ORDER MODEL

To obtain the complete P-box of output response of a structures or systems involving random and interval variables, it is necessary to perform random/interval UA at each realization/sample of the interval/random variables, which is normally time-consuming. Nevertheless, system responses at different realizations/samples of the interval/random variables are often correlated, which actually require only a small number of basis vectors to capture the largest part of the information they contain. This provides a possibility for constructing a ROM for hybrid UA with a much smaller number of simulation outputs.

ROM aims at constructing a low-dimensional representation of the simulation's responses defined on a basis which optimally spans the simulation's output space. A popular technique for finding such a basis is proper orthogonal decomposition (POD), which can provide an optimally ordered orthonormal basis in the least-squares sense from a relatively small set of simulation outputs (called snapshots) of the high-dimensional systems [17]. The optimal lower-dimensional representations for the given data are then obtained by truncating the optimal basis.

2.1. Proper orthogonal decomposition of the hybrid UA model

Consider the hybrid UA model in Eq.(1), if N_I realizations of the interval variables are obtained by discretization of Ω, $g(\boldsymbol{X},\boldsymbol{Z})$ is an N_I – dimensional output given by

$$\boldsymbol{Y} = \left[Y_1, Y_2, ..., Y_{N_I}\right]^{\mathrm{T}} \quad (3)$$

where $Y_i = g(\boldsymbol{X}, \boldsymbol{z}^{(i)}), i = 1,2,...,N_I$, and $\boldsymbol{z}^{(i)}$ is the *i*th realization of $\boldsymbol{Z}$. If N_R samples of the random variables are further generated according to their PDFs, an ensemble of simulation outputs or snapshots can be obtained as

$$\mathcal{Y} = \left[\boldsymbol{y}^{(1)}, \boldsymbol{y}^{(2)}, ..., \boldsymbol{y}^{(N_R)}\right] \quad (4)$$

where $\boldsymbol{y}^{(j)} = \left[y_1^{(j)}, y_2^{(j)}, ..., y_{N_I}^{(j)}\right]^{\mathrm{T}}, y_i^{(j)} = g(\boldsymbol{x}^{(j)}, \boldsymbol{z}^{(i)})$, $i = 1,2,...,N_I$, $j = 1,2,...,N_R$. $\mathcal{Y} \in \mathbb{R}^{N_I \times N_R}$ is a real-valued snapshot matrix of rank $N_Y \le \min\{N_I, N_R\}$. The POD representation of $g(\boldsymbol{X},\boldsymbol{Z})$ is based on the eigen-decomposition of $\mathcal{Y}$,i.e.,

$$\mathcal{Y}^{\mathrm{T}}\mathcal{Y}\boldsymbol{\psi} = \lambda\boldsymbol{\psi} \quad (5)$$

where $\mathcal{Y}^{\mathrm{T}}\mathcal{Y}$ is the correlation matrix of $g(\boldsymbol{X},\boldsymbol{Z})$. $\boldsymbol{\psi}$ and λ are eigenvector and eigenvalue of $\mathcal{Y}^{\mathrm{T}}\mathcal{Y}$. Each eigenvalue of $\mathcal{Y}^{\mathrm{T}}\mathcal{Y}$ represents the average energy captured by its corresponding eigenvector, and the total energy is given by the sum of the eigenvalues. The eigenvalue problem in Eq.(5) is related to the singular value decomposition (SVD) of matrix $\mathcal{Y}^{\mathrm{T}}$

$$\mathcal{Y}^{\mathrm{T}} = \boldsymbol{\Psi}\boldsymbol{\Sigma}\boldsymbol{V}^{\mathrm{T}}, \boldsymbol{\Sigma} = \begin{pmatrix} \boldsymbol{D} & \boldsymbol{0} \\ \boldsymbol{0} & \boldsymbol{0} \end{pmatrix} \quad (6)$$

where $\boldsymbol{D}$=*diagonal*$\left(\sigma_1, \sigma_2, ..., \sigma_{N_Y}\right)$ contains the singular values $\sigma_1 \ge \sigma_2 \ge ... \ge \sigma_{N_Y} \ge 0$ and zeros denote matrices of appropriate dimensions with zero-elements. $\boldsymbol{\Psi} \in \mathbb{R}^{N_R \times N_R}$ is the matrix of left singular vectors and $\boldsymbol{V} \in \mathbb{R}^{N_I \times N_I}$ is the matrix of right singular vectors. Both $\boldsymbol{\Psi} \in \mathbb{R}^{N_R \times N_R}$ and $\boldsymbol{V} \in \mathbb{R}^{N_I \times N_I}$ are unitary matrices with

$\boldsymbol{\Psi}\boldsymbol{\Psi}^{\mathrm{T}}=\boldsymbol{\Psi}^{\mathrm{T}}\boldsymbol{\Psi}=\boldsymbol{I}_{N_R}$ and $\boldsymbol{V}\boldsymbol{V}^{\mathrm{T}}=\boldsymbol{V}^{\mathrm{T}}\boldsymbol{V}=\boldsymbol{I}_{N_I}$. If $\boldsymbol{\psi}_i\in\mathbb{R}^{N_R}$ and $\boldsymbol{v}_i\in\mathbb{R}^{N_I}$ are the *i*th column vectors of $\boldsymbol{\Psi}$ and $\boldsymbol{V}$, respectively, $\{\boldsymbol{\psi}_i\}_{i=1}^{N_Y}$ and $\{\boldsymbol{v}_i\}_{i=1}^{N_Y}$ are eigenvectors of $\mathcal{Y}^{\mathrm{T}}\mathcal{Y}$ and $\mathcal{Y}\mathcal{Y}^{\mathrm{T}}$, respectively, with eigenvalues $\lambda_i=\sigma_i^2>0, i=1,...,N_Y$.

According to the Schimidt-Eckart-Young theory [18], the basis which consists of the first *L* left singular vectors of $\mathcal{Y}^{\mathrm{T}}$ minimizes the projection error of the snapshots among all *L*-dimensional orthogonal bases in $\mathbb{R}^{N_R}$. Therefore, the POD basis of *L* rank is just the first *L* columns of $\boldsymbol{\Psi}$. Based on the SVD decomposition in Eq.(6), the POD representation of $g(\boldsymbol{X},\boldsymbol{Z})$ can be defined as follows

$$Y=g(\boldsymbol{X},\boldsymbol{Z})\approx\sum_{i=1}^{L}c_i(\boldsymbol{z})\boldsymbol{\psi}_i(\boldsymbol{x}) \tag{7}$$

where $\{\boldsymbol{\psi}_i\}_{i=1}^{L}$ are the first *L* left singular vectors of $\mathcal{Y}^{\mathrm{T}}$, which are the most characteristic structure function extracted from the response space based on the snapshot matrix $\mathcal{Y}^{\mathrm{T}}$, $c_i(\boldsymbol{z})$ are the corresponding coefficients which are the functions of the interval variables $\boldsymbol{Z}$, and $L\in\{1,...,N_Y\}$ is the number of retained eigenvectors.

Since the square of the error of the POD representation in Eq. (7) is defined by the sum of the eigenvalues of the eigenvalue problem (5) which corresponds to the modes excluded in the selected basis, the number *L* of the POD basis can be selected according to the following criterion

$$\frac{\sum_{k=1}^{L}\lambda_k}{\sum_{k=1}^{N_Y}\lambda_k}>1-\varepsilon \tag{8}$$

where ε is a user-defined tolerance, which is often taken as 10^{-3} or smaller [14]. The numerator of Eq.(8) is normally referred to as the "energy" captured by the POD modes.

Clearly, for any realization $\boldsymbol{z}$ of interval variable, the corresponding response can be approximated with the POD representation in Eq.(7). The coefficients $c_i(\boldsymbol{z})$ of the POD are the functions of the interval variables $\boldsymbol{Z}$, it is, thus, possible to construct a mapping between the POD coefficients and the interval variables $\boldsymbol{Z}$. Theoretically, any surrogate model, such as polynomial chaos expansion, Kriging model and support vector machine, can be used for this purpose. In this paper, the choice is made to focus on Kriging model whose efficiency and accuracy for uncertainty propagation has been proved in many literatures [19].

2.2. Kriging model for the POD coefficients

Kriging is an exact interpolation metamodel. For a black-box function $c_i(\boldsymbol{z})$, the Kriging model function is expressed as:

$$c_{Ki}(\boldsymbol{Z})=\boldsymbol{f}^T(\boldsymbol{Z})\boldsymbol{\beta}+b(\boldsymbol{Z}) \tag{9}$$

where $\boldsymbol{f}^T(\boldsymbol{Z})\boldsymbol{\beta}$ is the deterministic part of the Kriging which gives an approximation of the response in mean. It represents the overall trend of the Kriging. In the regression model $\boldsymbol{f}^T(\boldsymbol{Z})\boldsymbol{\beta}$, $\boldsymbol{f}(\boldsymbol{Z})=\left[f_1(\boldsymbol{Z}),\cdots,f_q(\boldsymbol{Z})\right]^{\mathrm{T}}$ are the basis functions and $\boldsymbol{\beta}=\left[\beta_1,\cdots,\beta_q\right]^{\mathrm{T}}$ is the vector of regression coefficients, respectively. $b(\boldsymbol{Z})$ is a stationary Gaussian process with zero mean and covariance between two points of space as follows:

$$Cov\left[b(\boldsymbol{z}^{(i)}),b(\boldsymbol{z}^{(j)})\right]=\sigma^2R(\boldsymbol{z}^{(i)},\boldsymbol{z}^{(j)}) \tag{10}$$

where σ^2 is the process variance and $R(\cdot)$ is the correlation function. The anisotropic Gaussian correlation function is selected in this paper which can be formulated by

$$R(\boldsymbol{z}^{(i)},\boldsymbol{z}^{(j)})=\exp\left(-\sum_{m=1}^{n_I}\theta_m\left|z_m^{(i)}-z_m^{(j)}\right|^2\right) \tag{11}$$

where $z_m^{(i)}$ and $z_m^{(j)}$ are the *m*th coordinates of the points $\boldsymbol{z}^{(i)}$ and $\boldsymbol{z}^{(j)}$ and $\theta_m(m=1,\cdots,n_I)$ are the hyper-parameters which give the multiplicative inverse of the correlation length in different directions.

Given an initial design of experiments (DoE) $\left[\boldsymbol{z}^{(1)},\cdots,\boldsymbol{z}^{(N_I)}\right]^{\mathrm{T}}$ and the corresponding POD coefficients $\boldsymbol{C}_i=\left[c_i\left(\boldsymbol{z}^{(1)}\right),\cdots,c_i\left(\boldsymbol{z}^{(N_I)}\right)\right]^{\mathrm{T}}$, the unknown parameters $\boldsymbol{\beta}$ and σ^2 of Kriging model are estimated by the generalized least squares regression [20]

$$\boldsymbol{\beta} = (\mathcal{F}^T \mathcal{R}^{-1} \mathcal{F})^{-1} \mathcal{F}^T \mathcal{R}^{-1} \boldsymbol{C} \tag{12}$$

$$\sigma^2 = \frac{1}{N_I} (\boldsymbol{C} - \mathcal{F}\boldsymbol{\beta})^T \mathcal{R}^{-1} (\boldsymbol{C} - \mathcal{F}\boldsymbol{\beta}) \tag{13}$$

where $\mathcal{R}$ is the matrix of correlation with element at the *i*th row and *j*th column being $R(\boldsymbol{z}^{(i)}, \boldsymbol{z}^{(j)})(i, j = 1, \cdots, N_I)$, and $\mathcal{F} = \left[\boldsymbol{f}(\boldsymbol{z}^{(1)}), \cdots, \boldsymbol{f}(\boldsymbol{z}^{(N_I)}) \right]^T$ is the matrix of regression function.

The hyper-parameters $\theta_m (m = 1, \cdots, n_I)$ can be obtained by maximum likelihood estimation:

$$\boldsymbol{\theta} = \text{argmax} \left(-\frac{N_I}{2} \ln(\sigma^2) - \frac{1}{2} \ln(|\mathcal{R}|) \right) \tag{14}$$

Then, at an unobserved interval point $\boldsymbol{z}^{(*)}$, the POD coefficient predicted by the Kriging model and the corresponding variance can be given as [20]

$$c_i(\boldsymbol{z}^{(*)}) = \boldsymbol{f}^T(\boldsymbol{z}^{(*)})\boldsymbol{\beta} + \boldsymbol{r}^T(\boldsymbol{z}^{(*)}) \mathcal{R}^{-1} (\boldsymbol{C} - \mathcal{F}\boldsymbol{\beta}) \tag{15}$$

$$\sigma_c^2(\boldsymbol{z}^{(*)}) = \sigma^2 \left[1 - \boldsymbol{r}^T(\boldsymbol{z}^{(*)}) \mathcal{R}^{-1} \boldsymbol{r}(\boldsymbol{z}^{(*)}) + \left(\mathcal{F}^T \mathcal{R}^{-1} \boldsymbol{r}(\boldsymbol{z}^{(*)}) - \boldsymbol{f}(\boldsymbol{z}^{(*)}) \right)^T (\mathcal{F}^T \mathcal{R}^{-1} \mathcal{F})^{-1} \left(\mathcal{F}^T \mathcal{R}^{-1} \boldsymbol{r}(\boldsymbol{z}^{(*)}) - \boldsymbol{f}(\boldsymbol{z}^{(*)}) \right) \right] \tag{16}$$

where $\boldsymbol{r}(\boldsymbol{z}^{(*)}) = \left[R(\boldsymbol{z}^{(*)}, \boldsymbol{z}^{(1)}), \cdots, R(\boldsymbol{z}^{(*)}, \boldsymbol{z}^{(N_I)}) \right]^T$. Kriging is an exact interpolation method, and the Kriging prediction in a point of the design of experiments is exact with Kriging variance null. Therefore, Kriging variance enables to quantify the uncertainty of local predictions and provides a good index to improve a design of experiments.

2.3. Design of the experiment in the proposed method.

As explained in sections 2.1 and 2.2, a good DoE is necessary for both POD and Kriging. For POD, a proper set of snapshots have to be generated such that the space expanded by the POD basis extracted from snapshots can well approximate the hybrid UA model. For Kriging model, an appropriate number of interval realizations should be generated to get a convergent result under accuracy requirements.

According to the purpose of the hybrid UA in this paper, we aim at obtaining convergent P-box of the output response as well as its first two moments. Therefore, the number N_R of random samples is determined by the convergence of the output mean based on MCS [21], i.e.,

$$Cov_i = \sqrt{\frac{(1 - \mu_{Y_i})}{(N_R - 1)\mu_{Y_i}}}, i = 1, ..., N_I \tag{17}$$

where μ_{Y_i} is the estimated response mean at the *i*th realization of the interval variables based on N_R random samples, and Cov_i is the corresponding coefficient of the variation. If $\max_{i=1,\ldots,N_I} (Cov_i) < 0.1$, N_R is considered as sufficient.

For the number N_I of interval realizations, it has to be sufficient for extracting a good POD basis as well as constructing convergent Kriging model. For the former purpose, N_I has to be larger than N_Y. For the later purpose, the initial N_I should be larger than the minimum number of DoE required by the Kriging model, e.g. $N_I = (n_I + 1)(n_I + 2)/2$ for a 2nd order Kriging model used in this paper. Since N_I required for the later purpose is normally larger than that required for the former purpose, the initial N_I is chosen according to the later purpose, and then the convergence of the Kriging model is determined by the leave-one-out error [22].

3. ACADEMIC APPLICATIONS

Two examples are studied in this section to illustrate the accuracy of the proposed method, which is denoted as POD-Kriging. The estimated intervals for response mean and response variance as well as the P-box of response are compared to Crude MCS.

3.1. A planar 10-bar structure

The first example consists of a planar 10-bar structure as shown in Figure 2. The input variables are the length L of all the horizontal and the vertical bars, the elastic modulus E and the section area $A_i (i = 1, \cdots, 10)$ of all the bars. The left end of the structure is fixed, node 4 is subjected to a Y-direction load F_1, node 2 is subjected to an X-direction load F_2 and a Y-direction load F_3. The distribution types and parameters of the above input variables are shown in Table 1, where parameters 1 and 2 represent mean and standard

deviation for normal distribution, and represent lower and upper bounds for interval distribution.

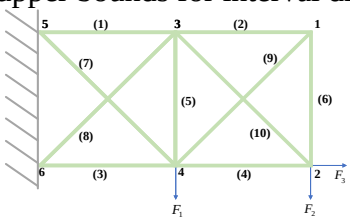

Figure 2:Diagram of the 10-bar structure.

Table 1:Distribution parameters of input variables

Variables	*Distribution type*	*Parameter 1*	*Parameter 2*
A_1~A_{10}/m^2	*Normal*	*0.001*	5×10^{-2}
L/m	*Interval*	*0.9*	*1.1*
F_1/N	*Interval*	7.5×10^{4}	9.5×10^{4}
F_2N	*Interval*	9×10^{3}	1.1×10^{4}
F_3/N	*Interval*	9×10^{3}	1.1×10^{4}
E/Pa	*Interval*	1.4×10^{10}	2.6×10^{10}

In this example, we consider the vertical displacement y, which can be calculated by:

$$y=(\sum_{i=1}^{6}\frac{N_i^0N_i}{A_i}+\sqrt{2}\sum_{i=7}^{10}\frac{N_i^0N_i}{A_i})\frac{L}{E}$$

In above equation, N_i^0 is the axial internal force of each bar when $F_1=F_3=0,F_2=1$. The internal force of bar 8 and bar 10 can be firstly obtained according to the nodal balance equation:

$$a_{11}N_8+a_{12}N_{10}=b_1 \qquad a_{21}N_8+a_{22}N_{10}=b_2$$

where

$$a_{11}=(\frac{1}{A_1}+\frac{1}{A_3}+\frac{1}{A_5}+\frac{2\sqrt{2}}{A_7}+\frac{2\sqrt{2}}{A_8})\frac{L}{2E}$$

$$a_{12}=a_{21}=\frac{L}{2A_5E}$$

$$b_1=(\frac{F_2}{A_1}-\frac{2F_2+F_1-F_3}{A_3}-\frac{F_2}{A_5}-\frac{2\sqrt{2}(F_2+F_1)}{A_7})\frac{\sqrt{2}L}{2E}$$

$$b_2=(\frac{\sqrt{2}(F_3-F_2)}{A_4}-\frac{\sqrt{2}F_2}{A_5}-\frac{4F_2}{A_9})\frac{L}{2E}$$

Thus, the internal forces of other bars can be obtained as follows:

$$N_1=F_2-\frac{\sqrt{2}}{2}N_8 \qquad N_2=-\frac{\sqrt{2}}{2}N_{10}$$

$$N_3=-F_1-2F_2+F_3-\frac{\sqrt{2}}{2}N_8 \qquad N_4=-F_2+F_3-\frac{\sqrt{2}}{2}N_{10}$$

$$N_5=-F_2-\frac{\sqrt{2}}{2}N_8-\frac{\sqrt{2}}{2}N_{10} \qquad N_6=-\frac{\sqrt{2}}{2}N_{10}$$

$$N_7=\sqrt{2}(F_1+F_2)+N_8 \qquad N_9=\sqrt{2}F_2+N_{10}$$

Table 2:Estimated intervals for response mean and variance

	MCS	*POD-Kriging*
$N(N_R\times N_I)$	*10544×10687*	*10544×47*
$[\mu_Y^L,\mu_Y^U]$	*[0.92544,2.27149] $\times10^{-2}$*	*[0.92709,2.71383] $\times10^{-2}$*
$[(\sigma_Y^2)^L,(\sigma_Y^2)^U]$	*[0.51161,4.36619] $\times10^{-7}$*	*[0.51083,4.37718] $\times10^{-7}$*
Cov_{max}	*0.10076*	*0.10067*

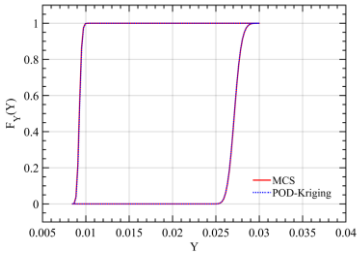

Figure 3:P-box of the response

According to the DoE strategy in section 2.3, we extracted 10544 samples of random variables according to their PDFs and 21 realizations of interval variables by discretization. As a result, we obtained a 10544×21-dimension real-valued snapshot matrix. After the SVD, we obtain a 10544×1-dimensional POD basis matrix and the corresponding POD coefficients. Based on the 21 initial realizations of interval variables and the corresponding POD coefficients, an initial POD-Kriging model is constructed which is then updated according to the leave-one-out method. Finally, 47 realizations of the interval variables are required by a convergent POD-Kriging model. The responses at 10687 realizations of the interval variables are then predicted by the established POD-Kriging model, based on which the intervals for the response mean and variance are estimated as shown in Table 2 (Cov_{max} is the maximum COV), and the P-box of responses is given in Figure 3. It can be seen that all the estimates of the proposed POD-Kriging method are in a good agreement with the corresponding references. However, the number of the realizations of interval variables required is significantly reduced in the proposed method.

3.2. A nonlinear Duffing oscillator

We consider a nonlinear Duffing oscillator which can simulate many nonlinear vibration problems in engineering practice, such as ship rolling motion, structural vibration, chemical bond destruction and so on. The control equation of the duffing oscillator is given by

$$\ddot{u}(t)+2\xi\omega\dot{u}(t)+\omega^2\left[u(t)+\varepsilon u^3(t)\right]=\zeta(A,w_x,t)$$

where $u(t)$ represents the displacement of the oscillator, ω represents natural frequency considering undamped linear structure, ξ represents damping ratio, and ε controls the nonlinearity of the system. $\zeta(A,w_x,t)$ is the excitation part of system which is expressed as $\zeta(A,w_x,t)=A\sin(w_x t)$, where A represents amplitude and w_x represents frequency.

The initial conditions are u=0, $\dot{u}$=0 and the problem is solved in the time domain [0, 10] s, with a time step of Δt=0.01s . The distribution types and parameters of input variables are shown in Table 3. The maximum absolute system output $y=\max\left|(u(t))\right|$ is the quantity of interest.

Table 3: Distribution parameters of input variables

Variables	*Distribution type*	*Parameter 1*	*Parameter 2*
ω	*Normal*	2π	0.2π
ζ	*Normal*	*0.03*	*0.003*
ε	*Normal*	*100*	*10*
A	*Interval*	*0.54*	*0.66*
w_x	*Interval*	*0.9*	*1.1*

Table 4:Estimated intervals for response mean and variance

	MCS	*POD-Kriging*
N ($N_R \times N_I$)	*6479×10201*	*6479×12*
$\left[\mu_Y^L,\mu_Y^U\right]$	*[1.53586,1.88397] ×10-2*	*[1.53533,1.88340] ×10-2*
$\left[(\sigma_Y^2)^L,(\sigma_Y^2)^U\right]$	*[0.88730,1.54106] ×10-5*	*[0.83672,1.48053] ×10-5*
$Cov_{\max}$	*0.09948*	*0.09949*

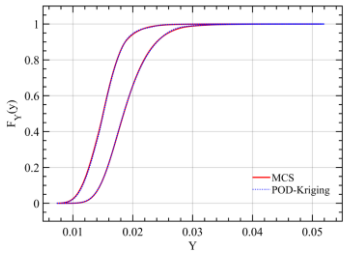

Figure 4:P-box of the response

This example is used to evaluate the performance of the POD-Kriging model for simulating the maximum absolute value of the dynamic system output. In this example, the final POD-Kriging model is constructed with 12 realizations of the interval variables. After SVD, from a 6479×12-dimension real-valued snapshot matrix we obtain a 6479×2-dimensional POD basis matrix and the corresponding POD coefficients. The final POD-Kriging model is then used to predict the responses at 10201 realizations of interval variables. The intervals for response mean and variance are obtained as shown in Table 4, while the estimated P-box of response is given in Figure 4. The comparison indicates that the proposed POD-Kriging model has good accuracy for simulating the maximum absolute value of the dynamic system output with significantly reduced computational cost. This has practical implications for reducing the cost of reliability analysis of dynamic systems with interval variables.

4. CONCLUSIONS

To reduce the computational cost of hybrid UA with both random and interval variables, a POD-Kriging model is established in the paper by borrowing the idea of reduced-order model. Two nonlinear examples are used to verify its efficiency and accuracy. The comparison with the Crude MCS method indicates that the proposed method can provide very good estimates not only for the intervals of the response mean and variance, but also for the P-box of the response with significantly reduced computational cost. Therefore, it should also provide an efficient way for reliability analysis of structures with hybrid random and interval variables, which will be further studied in the future. Besides, it is worth

mentioning that the focus in this paper is to improve the computational efficiency by reducing the number of the interval realizations. The criterion in Eq.(17) for determining the number of random samples is very conservative, which provides the possibility for further improving the efficiency of the proposed method.

5. ACKNOWLEDGEMENTS

This research was supported by the National Natural Science Foundation of China (Grant No. NSFC 51875464), which is gratefully acknowledged by the authors.

6. REFERENCES

[1] Coleman H W, Steele W G. Experimentation, validation, and uncertainty analysis for engineers[M]. *John Wiley & Sons*, 2018.

[2] Hurtado J E, Alvarez D A. The encounter of interval and probabilistic approaches to structural reliability at the design point[J]. *Computer Methods in Applied Mechanics and Engineering*, 2012, 225: 74-94.

[3] Xia B, Yu D. Response probability analysis of random acoustic field based on perturbation stochastic method and change-of-variable technique[J]. *Journal of Vibration and Acoustics*, 2013, 135(5):521–523.

[4] Sarrouy E, Dessombz O, Sinou J J. Piecewise polynomial chaos expansion with an application to brake squeal of a linear brake system[J]. *Journal of Sound and Vibration*, 2013, 332(3): 577-594.

[5] Qiu Z, Xia Y, Yang J. The static displacement and the stress analysis of structures with bounded uncertainties using the vertex solution theorem[J]. *Computer Methods in Applied Mechanics and Engineering*, 2007, 196(49-52): 4965-4984.

[6] Xia B, Yu D. Modified interval perturbation finite element method for a structural-acoustic system with interval parameters[J]. *Journal of Applied Mechanics*, 2013, 80(4): 041027.

[7] Lü H, Yu D. Brake squeal reduction of vehicle disc brake system with interval parameters by uncertain optimization[J]. *Journal of Sound and Vibration*, 2014, 333(26): 7313-7325.

[8] Ni B Y, Jiang C, Wu P G, et al. A sequential simulation strategy for response bounds analysis of structures with interval uncertainties[J]. *Computers & Structures*, 2022, 266: 106785.

[9] Gao W, Wu D, Song C, et al. Hybrid probabilistic interval analysis of bar structures with uncertainty using a mixed perturbation Monte-Carlo method[J]. *Finite Elements in Analysis and Design*, 2011, 47(7): 643-652.

[10] Xia B, Yu D, Liu J. Hybrid uncertain analysis of acoustic field with interval random parameters[J]. *Computer Methods in Applied Mechanics and Engineering*, 2013, 256: 56-69.

[11] Chen X, Qiu Z. A novel uncertainty analysis method for composite structures with mixed uncertainties including random and interval variables[J]. *Composite Structures*, 2018, 184: 400-410.

[12] Schöbi R, Sudret B. Structural reliability analysis for p-boxes using multi-level meta-models[J]. *Probabilistic Engineering Mechanics*, 2017, 48: 27-38.

[13] Li Q, Zhao N. A probability box representation method for power flow analysis considering both interval and probabilistic uncertainties[J]. *International Journal of Electrical Power & Energy Systems*, 2022, 142: 108371.

[14] Sun X, Pan X, Choi J I. Non-intrusive framework of reduced-order modeling based on proper orthogonal decomposition and polynomial chaos expansion[J]. *Journal of Computational and Applied Mathematics*, 2021, 390: 113372.

[15] Park K, Allen M S. A Gaussian process regression reduced order model for geometrically nonlinear structures[J]. *Mechanical Systems and Signal Processing*, 2023, 184: 109720.

[16] Xiao D, Fang F, Pain C C, et al. A parameterized non-intrusive reduced order model and error analysis for general time-dependent nonlinear partial differential equations and its applications[J]. *Computer Methods in Applied Mechanics and Engineering*, 2017, 317: 868-889.

[17] Algazi V, Sakrison D. On the optimality of the Karhunen-Loève expansion [J]. *IEEE Transactions on Information Theory*, 1969, 15(2): 319-321.

[18] Eckart C, Young G. The approximation of one matrix by another of lower rank[J]. *Psychometrika*, 1936, 1(3): 211-218.

[19] Echard B, Gayton N, Lemaire M, et al. A combined importance sampling and kriging reliability method for small failure probabilities with time-demanding numerical models[J].

Reliability Engineering & System Safety, 2013, 111: 232-240.

[20] Kleijnen J P C. Regression and Kriging metamodels with their experimental designs in simulation: A review[J]. *European Journal of Operational Research*, 2017, 256(1): 1-16.

[21] Liu J S. Monte Carlo strategies in scientific computing[M]. New York: springer, 2001.

[22] Liu H, Cai J, Ong Y S. An adaptive sampling approach for Kriging metamodeling by maximizing expected prediction error[J]. *Computers & Chemical Engineering*, 2017, 106: 171-182.